New Journal of Physics
The open–access journal for physics

Determination of the director profile in a nematic cell from guided wave data: an inverse problem

S L Cornford[1,3], T S Taphouse[1], C J P Newton[2] and J R Sambles[1]

[1] School of Physics, University of Exeter, Exeter EX4 4QL, UK
[2] HP Labs, Bristol, UK
E-mail: sc261@ex.ac.uk

New Journal of Physics **9** (2007) 166
Received 14 May 2007
Published 18 June 2007
Online at http://www.njp.org/
doi:10.1088/1367-2630/9/6/166

Abstract. We consider an inverse problem: the estimation of the nematic director profile from experimental fully leaky guided mode data. This inverse problem is ill-posed in that small changes in the data may lead to large changes in the estimates of the director profile. The continuum equations for a nematic are exploited to stabilize the problem. We use experimental data drawn from a study of the dynamics of a hybrid-aligned nematic cell as an example.

[3] Author to whom any correspondence should be addressed.

PII: S1367-2630(07)50397-6

Contents

1. Introduction

A one-dimensional liquid crystal cell, built from a thin layer of nematic material sandwiched between glass planes, is often used as an experimental model of the ubiquitous flat panel display device. The nematic layer is described by the director profile, a unit vector field $\boldsymbol{n}(z, t)$ which defines the average orientation of molecules within a small volume. The z-axis is normal to the nematic–glass interfaces. Both of the glass plates are coated on one side (adjacent to the liquid crystal) with indium tin oxide (ITO), a transparent conductor, to permit an electric potential to be applied across the cell, and treated in order to align the director at the interface. In a hybrid-aligned nematic (HAN) cell, the director is confined to the xz-plane, and varies from homeotropic alignment, parallel to the z-axis, at one surface to homogeneous alignment, parallel to the x-axis, at the other.

Physical theories of nematics typically allow the director to be calculated, provided that a set of phenomenological constants are known. The director within a liquid crystal cell is not directly visible, but specifies the dielectric tensor and so affects the external appearance of the device. While it is possible to predict this external appearance, using the Berreman 4×4 matrix method [1], once the director has been calculated, and hence test a given model against optical measurements, it is also useful to reconstruct the director assuming as little about its behaviour as possible. Examination of the reconstructed director helps the experimenter to decide which physical effects are important in a given cell, before testing specific models.

The fully-leaky guided mode experiment [2, 3] measures the optical transmission and reflection coefficients of a liquid crystal cell. In the context of inverse problem theory [4], the Berreman method is used to solve our *forward problem*, namely prediction of the experimental measurements given the dielectric tensor. Estimation of the dielectric tensor consistent with the experimental measurements by, for example, solving a least-squares problem, is an *inverse problem*, and more importantly is often an *ill-posed* problem. A singular value decomposition (SVD) analysis [5] shows that reconstruction of the dielectric tensor in steady-state is severely ill-posed, and so additional information is required.

When a uniaxial liquid crystal is studied, the dielectric tensor is determined by $\boldsymbol{n}(z, t)$ and the complex permittivities $\epsilon_\perp$ and $\epsilon_\parallel$. In a HAN cell, the director can be characterized solely

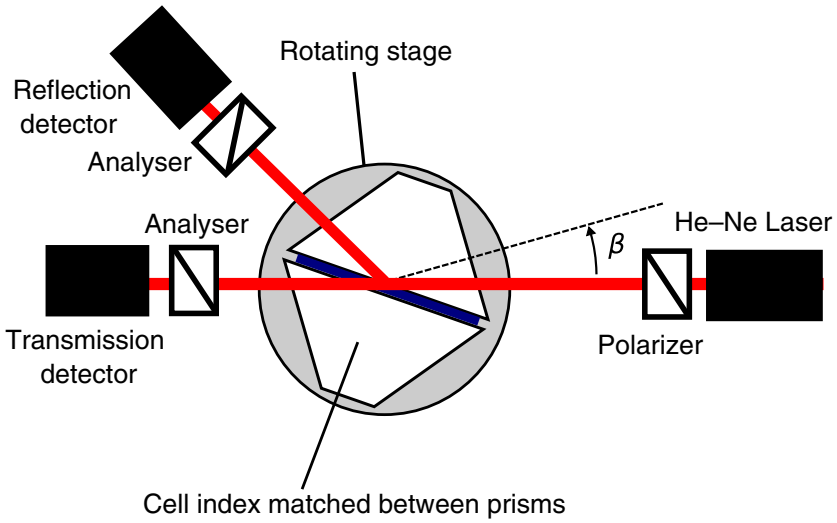

Figure 1. The fully-leaky guided-mode experiment apparatus. The angle β between the incident beam and the normal to the first prism face is varied, allowing the reflection and transmission coefficients to be measured as a function of β.

by the director tilt angle $\theta(z, t)$, defined in this paper as the angle between the director and the z-axis. Despite these simplifications the least-squares problem remains ill-posed, so that even the smallest experimental error prevents reconstruction of the director. SVD analysis, together with a consideration of the Ericksen–Leslie theory of nematodynamics, leads us to propose and test an improved inverse problem.

2. Experimental details

The time-resolved fully-leaky guided-mode experiment shown in figure 1 is designed to detect changes in the director with sub-millisecond resolution. Operation of this experiment is quite complex, and so is outlined below.

A liquid crystal cell is coated with index matching fluid and set between glass prisms, then the resulting assembly is mounted on a rotating table so that the prism faces are parallel to the laboratory y-axis. The polarizer and analysers are set to select either s- or p-polarized light and the rotating table set to an initial angle $\beta = \beta_0$. A time-dependent electric potential, $v_0(t)$, is applied across the cell, and the reflection coefficient, R, and transmission coefficient, T, measured as a function of time. These time-dependent measurements are repeated for a range of angles $\beta \in \{\beta_0, \ldots, \beta_n\}$, and for each permutation of polariser and analyser states. For each time and angle, eight signals R_{pp}, R_{ps}, R_{sp}, R_{ss}, T_{pp}, T_{ps}, T_{sp} and T_{ss} are recorded, where the first subscript denotes the state of the polarizer, and the second subscript denotes the state of the analyser. The collected data are sorted into a vector

$$\boldsymbol{b} = (\boldsymbol{b}_0^T, \boldsymbol{b}_1^T, \ldots, \boldsymbol{b}_m^T)^T, \tag{1}$$

where the sub-vectors $\boldsymbol{b}_j$ are constructed from data recorded at times t_j relative to the start of the pulse,

$$\boldsymbol{b}_j = (R_{\mathrm{pp}}(\beta_0, t_j), R_{\mathrm{pp}}(\beta_1, t_j), \ldots, R_{\mathrm{pp}}(\beta_n, t_j), R_{\mathrm{ps}}(\beta_0, t_j), \ldots, T_{\mathrm{ss}}(\beta_n, t_j))^T. \tag{2}$$

The cell studied in this paper is a 3 μm thick HAN cell filled with Merck ZLI-4788-000, a material whose preferred alignment direction is perpendicular to a low-frequency electric field. To make the homogeneous surface, Nissan 150 polyimide was spin-coated onto ITO-coated glass, which was then baked at 450 K for 1 hour and rubbed to promote an alignment direction (and hence define the cell x-axis). A proprietary treatment supplied by Merck was used to produce a homeotropic surface.

3. Ericksen–Leslie theory

A short review of the Ericksen–Leslie theory of nematic materials appropriate to HAN cells [6]–[8] is needed before the forward and inverse problems can be analysed. The state variables are the tilt $\theta(z, t)$, the x-component of the flow velocity $u(z, t)$, and the electric potential $v(z, t)$. Since the flow is assumed incompressible, the z-component of the flow is zero, while the y-component of the flow is zero because all rotations of the director, and hence torques, are confined to the xz-plane. Inertial terms in the equations for the balance of linear and angular momenta are neglected, as they are assumed to relax on short timescales compared to re-alignment of the director in typical, thin cells.

The electric potential in the cell is calculated from Gauss' law,

$$\frac{\partial}{\partial z}\left(\epsilon_0\left(\epsilon_{\mathrm{a}}\cos^2\theta + \epsilon_\perp\right)\frac{\partial v}{\partial z}\right) = 0. \tag{3}$$

$v(z, t)$ may be the RMS amplitude of an alternating potential, in which case it is assumed that the frequency f is sufficiently large that resulting fluctuations in the director alignment can be neglected. Both of the permittivities $\epsilon_\perp$ and $\epsilon_\parallel$, and hence $\epsilon_{\mathrm{a}} = \epsilon_\parallel - \epsilon_\perp$, depend upon temperature and f. For ZLI-4788-000 at $f = 1$ kHz and at a temperature of 20 °C the manufacturer provides the values $\epsilon_\perp = 10.2$ and $\epsilon_\parallel = 4.5$ (so that $\epsilon_{\mathrm{a}} = -5.7$).

The x-component of the conservation of linear momentum equation is

$$\frac{\partial}{\partial z}\left(h(\theta)\frac{\partial u}{\partial z} - (\alpha_3\sin^2\theta - \alpha_2\cos^2\theta)\frac{\partial\theta}{\partial t}\right) = 0, \tag{4}$$

where

$$h(\theta) = \tfrac{1}{2}(\alpha_4 + \alpha_5 + 2\alpha_3\sin^2\theta + \alpha_2(\sin^2\theta - \cos^2\theta) + \alpha_1\cos^2\theta\sin^2\theta). \tag{5}$$

The six coefficients α_k are the Leslie viscosities, reduced to five by the Parodi relation $\alpha_6 - \alpha_5 = \alpha_2 + \alpha_3$. Like the permittivities, the viscosities are temperature dependent. Merck only supply a value (309 mPa s at 20 °C) for the rotational viscosity $\gamma_1 = \alpha_3 - \alpha_2$; one of the ultimate aims of our experiment is to determine the remaining viscosities. Since α_4 and α_5 only appear in the equations above as the combination $\alpha_4 + \alpha_5$, we cannot expect to determine these

viscosities individually. A set of inequality constraints on the Leslie viscosities ensure that energy dissipation is positive definite. In an untwisted, one-dimensional cell, such as a HAN cell:

$$\gamma_1 \geqslant 0, \tag{6}$$

$$2(\alpha_4 + \alpha_5) + \alpha_2 + \alpha_3 \geqslant 0, \tag{7}$$

$$\alpha_1 + 2(\alpha_4 + \alpha_5) + \alpha_2 + \alpha_3 \geqslant 0, \tag{8}$$

$$\gamma_1 \left(2(\alpha_4 + \alpha_5) + \alpha_2 + \alpha_3\right) - (\alpha_2 + \alpha_3)^2 \geqslant 0. \tag{9}$$

The equation for the conservation of angular momentum is

$$\left(k_{11}\sin^2\theta + k_{33}\cos^2\theta\right)\frac{\partial^2\theta}{\partial z^2} + (k_{11} - k_{33})\sin\theta\cos\theta\left(\frac{\partial\theta}{\partial z}\right)^2 - \epsilon_0\epsilon_a\sin\theta\cos\theta\left(\frac{\partial v}{\partial z}\right)^2 - \gamma_1\frac{\partial\theta}{\partial t} - (\alpha_3\sin^2\theta - \alpha_2\cos^2\theta)\frac{\partial u}{\partial z} = 0, \tag{10}$$

where k_{11} and k_{33} are the splay and bend elastic constants respectively. Merck give the values $k_{11} = 13.7$ pN and $k_{33} = 18.9$ pN at 20 °C.

Equations (3), (4) and (10) must be solved together with appropriate boundary conditions. Strong anchoring at the cell walls, located at $z = 0$ and $z = d$, is assumed, so the boundary values $\theta(0, t) = \theta_0$ and $\theta(d, t) = \theta_d$ do not change with time. The electric potential difference $v_0(t)$ is known, and since the model is unchanged by the addition of a constant to $v(z, t)$, we set $v(0, t) = v_0(t)$ and $v(d, t) = 0$. No-slip conditions are imposed on the flow: $u(0, t) = u(d, t) = 0$. Initial values $\theta(z, 0)$, $v(z, 0) = 0$ and $u(z, 0) = 0$ are given by the steady state solution to equations (3), (4) and (10) when no electric field is applied.

A useful simplification, the one-constant approximation, can be made to (10) by setting $k_{11} = k_{33} = k$, where k is given, for example, by the mean of the supplied values of k_{11} and k_{33}. If flow is also neglected, and no electric field is applied,

$$k\frac{\partial^2\theta}{\partial z^2} - \gamma_1\frac{\partial\theta}{\partial t} = 0. \tag{11}$$

If, at $t = 0$, the tilt profile is expressed as a sum of a linear tilt profile and a Fourier series

$$\theta(z, 0) = \theta_0 + \frac{(\theta_d - \theta_0)}{d}z + \sum_{n=1}^{n=\infty} b_n \sin(n\pi z), \tag{12}$$

then the solution to (11) is:

$$\theta(z, t) = \theta_0 + \frac{(\theta_d - \theta_0)}{d}z + \sum_{n=1}^{n=\infty} b_n \exp\left(-\frac{kn^2t}{\gamma_1}\right)\sin(n\pi z). \tag{13}$$

This solution expresses the most basic time-dependent behaviour of the liquid crystal: in steady-state the director varies smoothly (and in the one-constant case, linearly) with z, while any spatial oscillation in the director decays at a rate which increases rapidly with its wavenumber.

4. The forward problem

Berreman's 4×4 matrix method treats the propagation of light through stratified, anisotropic media, such as a simple liquid crystal cell, accounting for both transmission and reflection. In this system, Maxwell's equations are reduced to four linear differential equations in the wave amplitudes $\boldsymbol{\psi} = (E_x(z), H_y(z), E_y(z), -H_x(z))^T$, and may be expressed in a matrix-vector form,

$$\frac{\partial}{\partial z}\boldsymbol{\psi} = \frac{\mathrm{i}\omega}{c}\boldsymbol{\Delta}\boldsymbol{\psi}. \tag{14}$$

The matrix $\boldsymbol{\Delta}$ depends on the dielectric tensor, the internal angle (the angle of incidence at the prism-sample interface) and the refractive index of the glass prism. The general solution to (14) is

$$\boldsymbol{\psi}(z) = \boldsymbol{P}\boldsymbol{\psi}(z_0), \tag{15}$$

when the initial values $\boldsymbol{\psi}(z_0)$ are known. Equation (15) can be re-arranged to give the coefficients $R'_{\mathrm{pp}}, \ldots, T'_{\mathrm{ps}}$ at the prism-sample interface as a function of internal angle (see for example the appendix of [5]). Snell's law and Fresnel's equations are sufficient to convert $R'_{\mathrm{pp}}, \ldots, T'_{\mathrm{ps}}$ into the measured coefficients $R_{\mathrm{pp}}, \ldots, T_{\mathrm{ps}}$ as a function of external angle.

The matrix $\boldsymbol{P}$ is called the characteristic matrix of the region $[z_0, z]$. Over a homogeneous region of thickness h, the characteristic matrix is given by a simple expression:

$$\boldsymbol{P} = \exp\left(\mathrm{i}\frac{2\pi}{\lambda h}\boldsymbol{\Delta}\right) = \boldsymbol{I}_4 + \mathrm{i}\frac{2\pi h}{\lambda}\boldsymbol{\Delta} - \left(\frac{2\pi h}{\lambda}\right)^2 \frac{\boldsymbol{\Delta}\boldsymbol{\Delta}}{2!} - \cdots. \tag{16}$$

Several numerical techniques exist in which an inhomogeneous region is approximated by many thin, homogeneous layers. The general solution (15) can be rewritten in terms of n layers,

$$\boldsymbol{\psi}(z_n) = \boldsymbol{P}_n\boldsymbol{\psi}(z_{n-1}) = \boldsymbol{P}_n\boldsymbol{P}_{n-1}\ldots\boldsymbol{\psi}(z_0). \tag{17}$$

Each of the matrices $P_1, P_2, \ldots, P_n$ is calculated by an expression equivalent to (16). Wohler [9] used the theorem of Cayley and Hamilton to reduce the infinite series (16) to an expression of fourth-order in $\boldsymbol{\Delta}$ and its eigenvalues. Since explicit expressions are available for the eigenvalues of $\boldsymbol{\Delta}$ when the dielectric tensor is uniaxial, this implementation is numerically efficient. Ko [10] employed a scattering matrix formalism, primarily to avoid numerical difficulties associated with total internal reflection. The scattering matrix method requires the eigenvalues and eigenvectors of $\boldsymbol{\Delta}$, and involves calculation of the inverse of a 4×4 matrix, for each layer. It is clear from (16) that the characteristic matrix of any layer tends to the 4×4 identity matrix $\boldsymbol{I}_4$ as $h/\lambda \to 0$. This implies that even a large amplitude perturbation to the dielectric tensor leads to only a small change to the optical coefficients, if it is limited to a thin region, and therefore we expect our experiment to be sensitive just to broad features in the director profile.

In a HAN cell filled with a uniaxial nematic material, such as ZLI-4788-000, the dielectric tensor is determined by the director tilt $\theta(z, t)$ and the two complex dielectric constants $\epsilon_{\parallel}$ and $\epsilon_{\perp}$. In the simplest numerical treatment $\theta(z, t)$ would be built from the mean tilt angle in each of n layers. Instead, since we expect the director to be approximately described by the continuum

model, we compute $\bar{\theta}(z, t)$ by solving (10) and (3) numerically, neglecting flow and using the values supplied by Merck for k_{11}, k_{33} etc, and set

$$\theta(z, t) = \bar{\theta}(z, t) + x(z, t). \tag{18}$$

The vector

$$\boldsymbol{x} = (\boldsymbol{x}_0^T, \boldsymbol{x}_1^T, \ldots, \boldsymbol{x}_m^T)^T \tag{19}$$

is a discrete representation of $x(z, t)$, where the components of each sub-vector $\boldsymbol{x}_j$ are the corrections to the director profile in each layer at time t_j:

$$\boldsymbol{x}_j = (x(z_0, t_j), x(z_1, t_j), \ldots, x(z_n, t_j)). \tag{20}$$

The results of the Berreman calculation for a given subvector $\boldsymbol{x}_j$, denoted $\boldsymbol{f}_{\mathrm{B}}(\boldsymbol{x}_j)$, are sorted in the same order as the data vector (1), allowing the forward problem to be represented as a vector function

$$\boldsymbol{f}(\boldsymbol{x}) = \left(\boldsymbol{f}_{\mathrm{B}}(\boldsymbol{x}_0), \boldsymbol{f}_{\mathrm{B}}(\boldsymbol{x}_1), \ldots, \boldsymbol{f}_{\mathrm{B}}(\boldsymbol{x}_m)\right). \tag{21}$$

We will consider two similar inverse problems: a steady-state problem (where $m = 0$), in which we attempt to recover the initial tilt profile, and a time-dependent problem.

5. The inverse problem

We assume that errors in the experimental data are Gaussian, and that $\boldsymbol{f}(\boldsymbol{x})$ is only weakly nonlinear. This allows us to formulate a nonlinear least-squares problem: find $\boldsymbol{x}$ which minimizes the objective function

$$\Phi(\boldsymbol{x}) = \|\boldsymbol{f}(\boldsymbol{x}) - \boldsymbol{b}\|_2^2. \tag{22}$$

The 2-norm of a vector $\boldsymbol{v}$ is defined by $\|\boldsymbol{v}\|_2 = \sqrt{\boldsymbol{v}^T\boldsymbol{v}}$. The Gauss–Newton method is used to compute a sequence of vectors $\boldsymbol{x}_k$, where

$$\boldsymbol{x}_{k+1} = \boldsymbol{x}_k + (\boldsymbol{J}^T\boldsymbol{J})^{-1}\boldsymbol{J}^T(\boldsymbol{f}(\boldsymbol{x}_k) - \boldsymbol{b}). \tag{23}$$

The Jacobian matrix $\boldsymbol{J}$ is the matrix of partial derivatives of $\boldsymbol{f}$ with respect to $\boldsymbol{x}$,

$$J_{ij} = \frac{\partial f_i}{\partial x_j}. \tag{24}$$

If the method works as intended, both the objective function and the size of the Gauss–Newton update, $\|\boldsymbol{x}_{k+1} - \boldsymbol{x}_k\|_2$, should decay rapidly with the iteration number, k. In our case, the ill-posed nature of the problem will prevent the Gauss–Newton method from converging, or will cause it to converge to a spurious solution.

Singular value decomposition is widely used in the analysis of ill-posed problems, and will be used here to show why the unmodified Gauss–Newton method is expected to fail in our case. Any rectangular matrix, such as $\boldsymbol{J}$, may be expressed as an SVD:

$$\boldsymbol{J} = \boldsymbol{U}\boldsymbol{S}\boldsymbol{V}^T. \tag{25}$$

$\boldsymbol{S}$ is a diagonal matrix; its components $S_{jj} = \sigma_j$ are known as singular values, are non-negative, and are conventionaly ordered such that $\sigma_j \leqslant \sigma_{j-1}$. The matrices $\boldsymbol{U}$ and $\boldsymbol{V}$ are orthonormal; their columns $\boldsymbol{u}_j$ and $\boldsymbol{v}_j$ are respectively called left and right singular vectors. For a typical ill-posed problem the singular values σ_j decay continuously as j increases, while the number of sign changes in the components of $\boldsymbol{u}_j$ and $\boldsymbol{v}_j$ grows. Rewriting the Gauss–Newton method in terms of the SVD,

$$\boldsymbol{x}_{k+1} = \boldsymbol{x}_k + \sum_j \frac{1}{\sigma_j}\boldsymbol{v}_j\boldsymbol{u}_j^T(\boldsymbol{f}(\boldsymbol{x}_k) - \boldsymbol{b}). \tag{26}$$

Unless $\boldsymbol{u}_j^T(\boldsymbol{f}(\boldsymbol{x}_k) - \boldsymbol{b})$ decreases faster as j increases than σ_j does, the contribution of $\boldsymbol{v}_j$ to the update will increase with j. A problem in which $\boldsymbol{u}_j^T(\boldsymbol{f}(\boldsymbol{x}_k) - \boldsymbol{b})$ does decay quickly enough is said to satisfy the discrete Picard condition [11, 12]. The discrete Picard condition is usually violated for an ill-posed problem if $\boldsymbol{b}$ includes randomly distributed error, which is represented similarly in each $\boldsymbol{u}_j^T\boldsymbol{b}$.

Figure 2 shows that the steady-state inverse problem does not satisfy the discrete Picard condition. The coefficients of $\boldsymbol{v}_j$ for the first Gauss–Newton update, $c_j = \boldsymbol{u}_j^T(\boldsymbol{f}(0) - \boldsymbol{b})/\sigma_j$, were calculated for three data vectors: firstly a vector of noiseless synthetic data where $\boldsymbol{b}_\mathrm{s} = \boldsymbol{f}(a\sin(\pi z/2d))$, secondly a vector of noisy synthetic data $\boldsymbol{b}_\mathrm{r} = \boldsymbol{f}(0) + \boldsymbol{e}$, where the components of $\boldsymbol{e}$ are pseudo-random samples from the normal error distribution, and finally experimental data $\boldsymbol{b}_\mathrm{e}$. As j increases, the coefficients c_j calculated from $\boldsymbol{b}_\mathrm{r}$ and $\boldsymbol{b}_\mathrm{e}$ increase far more quickly than the coefficients calculated from $\boldsymbol{b}_\mathrm{s}$. Simply put, as j increases the growth of the coefficients c_j computed for the real data is dominated by experimental error. The consequences for our inverse problem are severe: at each iteration of (26) the presence of experimental error causes the update to be dominated, in an entirely spurious manner, by vectors $\boldsymbol{v}_j$ having many sign changes. Since $\boldsymbol{J}$ changes with $\boldsymbol{x}$, we cannot expect the iterations to converge; even if $\boldsymbol{J}$ were constant we would recover a noisy tilt profile.

5.1. Tikhonov regularization

Tikhonov regularization is frequently used to stabilize ill-posed problems. A side constraint is added to the objective function, so that

$$\Phi(\boldsymbol{x}) = \|\boldsymbol{f}(\boldsymbol{x}) - \boldsymbol{b}\|_2^2 + \lambda^2\|\boldsymbol{L}\boldsymbol{x}\|_2^2, \tag{27}$$

leading to a modified Gauss–Newton formula:

$$\boldsymbol{x}_{k+1} = \boldsymbol{x}_k + \sum_j \frac{\sigma_j}{\sigma_j^2 + \lambda^2}\boldsymbol{v}_j\boldsymbol{u}_j^T(\boldsymbol{f}(\boldsymbol{x}) - \boldsymbol{b}), \tag{28}$$

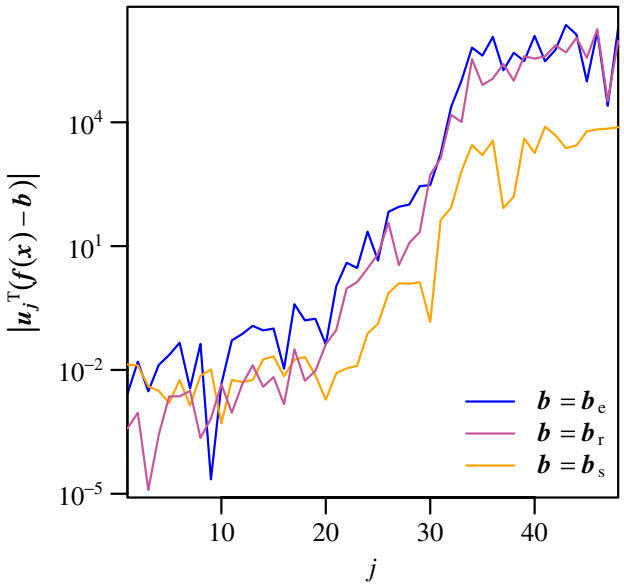

Figure 2. The coefficients $c_j = \boldsymbol{u}_j^T(\boldsymbol{f}(\boldsymbol{0}) - \boldsymbol{b})/\sigma_j$ for the steady-state inverse problem. When $\boldsymbol{b} = \boldsymbol{b}_s$, the noiseless synthetic data, the coefficients increase with j, but the rate of increase is even greater when $\boldsymbol{b} = \boldsymbol{b}_r$, the noisy synthetic data. The coefficients calculated when $\boldsymbol{b} = \boldsymbol{b}_e$, the experimental data, grow at a similar rate to those calculated from the noisy synthetic data.

where the new SVD is related to the Jacobian matrix by the formula

$$\boldsymbol{USV}^T = \boldsymbol{JL}^{-1}. \tag{29}$$

The matrix $\boldsymbol{L}$ and the *regularization parameter* λ impose some kind of prior knowledge on the solution. The objective function (27) can be derived from Bayes theorem assuming a Gaussian prior probability density with the covariance matrix $\lambda^2/e^2\boldsymbol{L}^T\boldsymbol{L}$, where e^2 is the variance of the noise in $\boldsymbol{b}$. Since we do not have such precise prior knowledge we select $\boldsymbol{L}$ by considering the Ericksen–Leslie equations and seek λ such that the discrete Picard condition is satisfied. When $\lambda = 0$, the original method (26) is recovered, while if λ is large we simply solve $\boldsymbol{Lx} = 0$. For intermediate values of $\lambda \sim \sigma_j$, the contributions of the $\boldsymbol{v}_j$ to the solution are progressively filtered out as j increases.

Choosing the identity matrix for $\boldsymbol{L}$ is equivalent to assuming that $\boldsymbol{x}$ is close to zero, in the sense that $\|\boldsymbol{x}\|_2$ is small, and so at first glance might seem appropriate for our problem. A SVD analysis of the steady-state inverse problem suggests otherwise. Figure 3(a) shows the first eight right singular vectors $\boldsymbol{v}_j$ of $\boldsymbol{J}$. None of the $\boldsymbol{v}_j$ are smooth, so it will be impossible to construct a smooth tilt profile from them, whatever the value of λ. An alternative choice of $\boldsymbol{L}$ is derived from the continuum model, with the intention that the physics contained in (11) should be weakly imposed upon the inverse problem. First, a vector

$$\boldsymbol{g}(\boldsymbol{x}) = (\boldsymbol{g}_0^T(\boldsymbol{x}), \boldsymbol{g}_1^T(\boldsymbol{x}), \ldots, \boldsymbol{g}_m^T(\boldsymbol{x})) \tag{30}$$

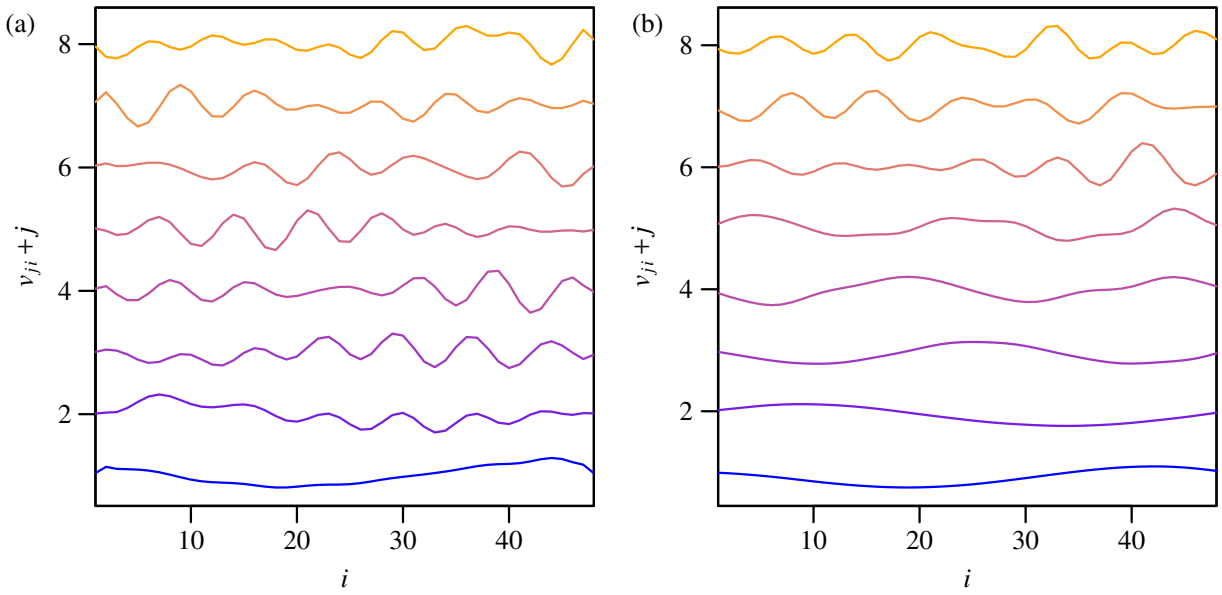

Figure 3. (a) Right singular vectors of $\boldsymbol{J}$. The first 8 of 48 vectors are shown, offset vertically by j for clarity. (b) Right singular vectors of $\boldsymbol{JL}^{-1}$ from the regularized problem. The frequency of oscillations in v_j with respect to z increases slowly with j.

is defined, where the ith element of the sub-vector $\boldsymbol{g}_j(\boldsymbol{x})$, $g_{ji}(\boldsymbol{x})$, is equal to the left-hand side of (11) evaluated in the ith layer:

$$g_{ji}(\boldsymbol{x}) = k\frac{\partial^2 x}{\partial z^2}(z_n, t_j) - \gamma_1 \frac{\partial x}{\partial t}(z_n, t_j). \tag{31}$$

The space- and time-derivatives are evaluated using difference formulae, then a square matrix $\boldsymbol{L}$ is built from the elements

$$L_{kl} = \frac{\partial g_k}{\partial x_l}. \tag{32}$$

The vector $\boldsymbol{g}(\boldsymbol{x})$ is linear with respect to $\boldsymbol{x}$, i.e. $\boldsymbol{g}(\boldsymbol{x}) = \boldsymbol{Lx}$, thus the objective function (27) represents a trade-off, governed by the value of λ, between goodness of fit to experimental data and our simple description of nematodynamics. For the steady-state inverse problem the number of sign changes in the right singular vectors of $\boldsymbol{JL}^{-1}$ (figure 3(b)) increases monotonically with j, so we expect solutions to be smooth if λ is large enough. Similarly, we expect to find time-dependent solutions where any spatial oscillations decay with time, at a rate which increases with their frequency.

5.2. Solutions to the steady-state inverse problem

To reduce the number of parameters in our problem, and hence reduce computational time, $x(z, t)$ is approximated by values on a coarse grid. The Berreman calculation must be performed using a relatively fine mesh to satisfy the assumption that the dielectric tensor is nearly constant within each layer. Since the director is expected to vary smoothly, cubic spline interpolation is used to calculate values of $x(z, t)$ at each point on the fine grid given the values at points on the coarse grid.

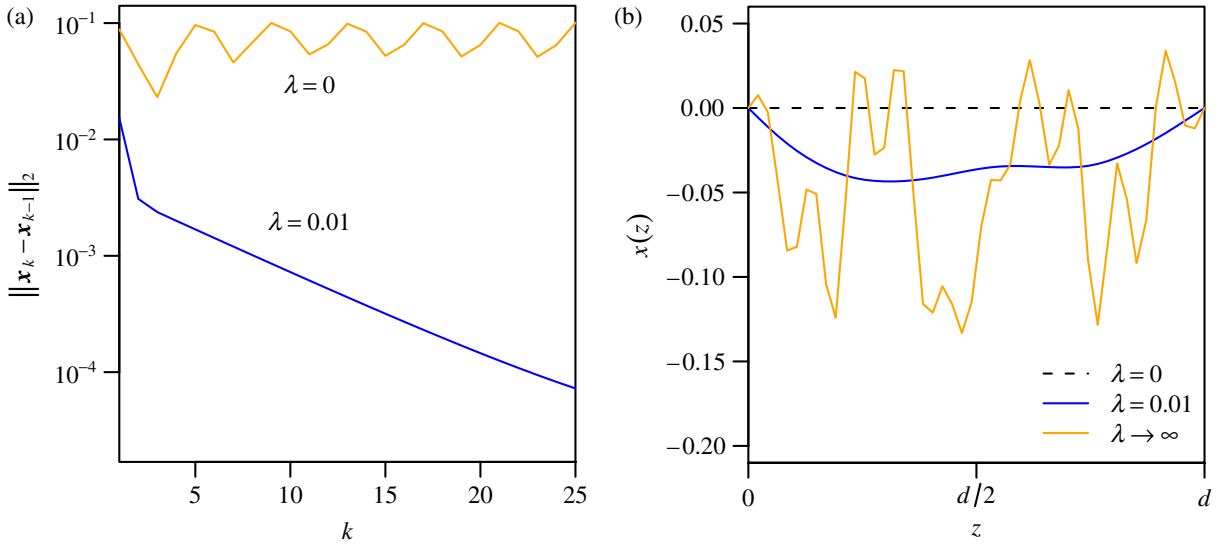

Figure 4. (a) Length of the Gauss–Newton step against iteration number. For the unregularized problem, where $\lambda = 0$, the sequence x_k does not converge. When the problem is regularised ($\lambda = 0.01$), the behaviour of x_k is improved. (b) $x(z, 0)$ for different λ. When $\lambda = 0$, a solution with high frequency oscillations in z is recovered. When $\lambda = 0.01$, a non-trivial solution is found in which oscillations are damped. When $\lambda \to \infty$ (dotted line), $x(z, 0) = 0$.

Solutions to the steady-state inverse problems were found for several values of λ, using a coarse grid of 20 layers and a fine grid of 48 layers. Three cases, $\lambda = 0$, $\lambda = 0.01$, and $\lambda \to \infty$ (when we simply minimize $\|\boldsymbol{Lx}\|_2^2$) serve to illustrate the effect of varying this parameter. The solution when $\lambda \to \infty$ is simply the trivial solution $\boldsymbol{x} = 0$. When the inverse problem is not regularized ($\lambda = 0$) the size of the update, $\|\boldsymbol{x}_k - \boldsymbol{x}_{k-1}\|_2$, remains roughly constant, at around 10^{-1}, beyond the fifth iteration, as shown in figure 4(a). Each new generation of the director profile features large amplitude oscillations across the cell, while the positions of the peaks and troughs change with every iteration. Figure 4(b) shows one of these noisy tilt profiles, each one of which fits the experimental data rather well, as can be seen in the $t = 0$ ms curves in figure 5(c). When the coarse grid has more than 24 layers the updates at each iteration grow exponentially. When $\lambda = 0.01$, the Gauss–Newton updates decay in magnitude to less than 10^{-4} after 25 iterations. Oscillations in the final tilt profile are damped compared to the case $\lambda = 0$, while the fit to the data is only marginally worse.

5.3. Solutions to the time-dependent inverse problem

The inverse problem was solved for experimental data taken during a 64 ms period after a 3 V ac potential was applied across the HAN cell. Without regularization, the Gauss–Newton iterations do not converge, just as in the steady-state case. In addition to the spatial oscillations seen previously, successive tilt profiles cross in a seemingly random fashion, so that no trend further than gross motion from one equilibrium to another can be discerned (figure 5(a)). Figure 5(c) shows that the reflection and transmission coefficients calculated from these clearly unphysical tilt profiles are in good agreement with the experimental data.

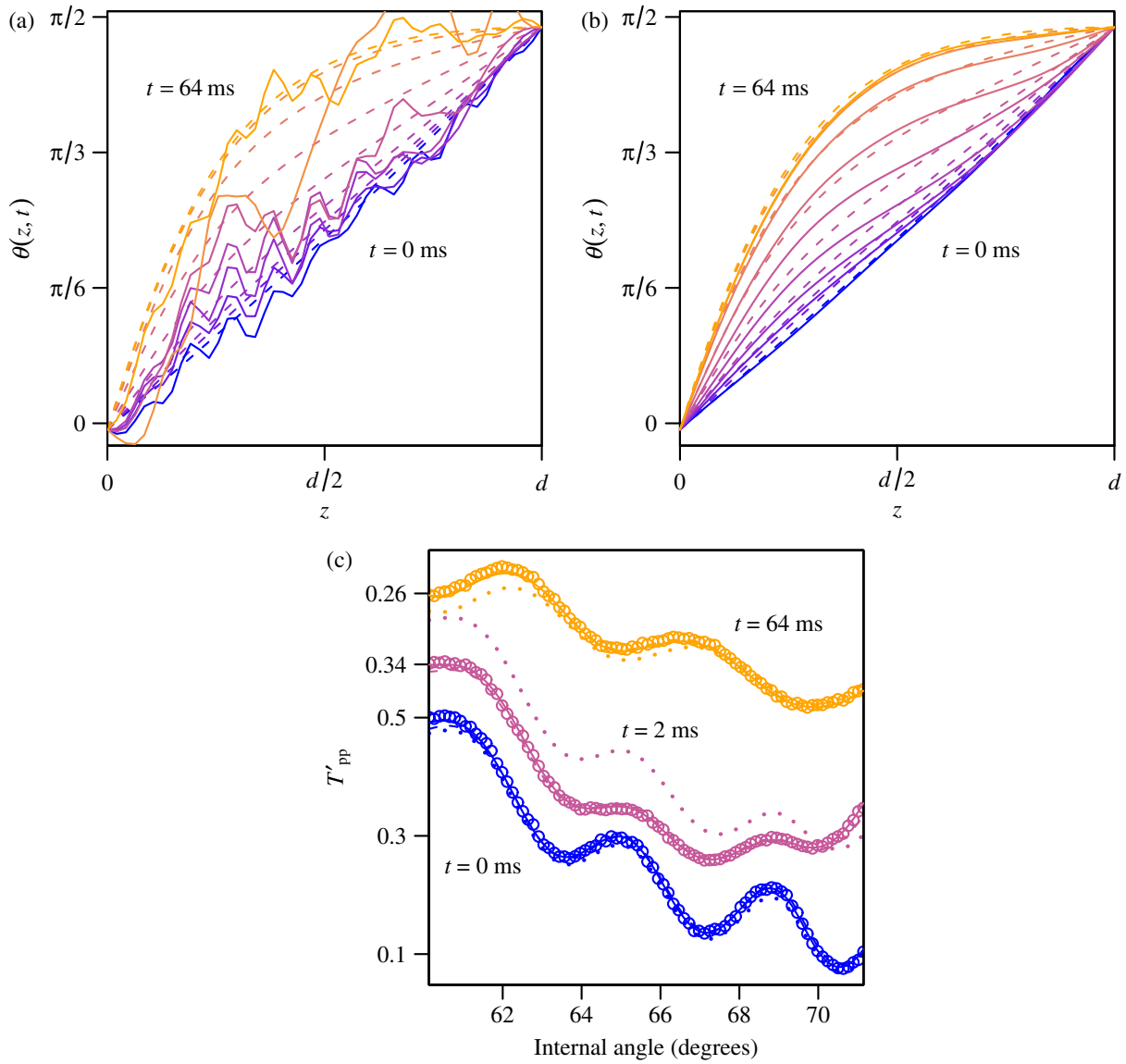

Figure 5. Solutions to the time-dependent inverse problem (a) unregularized solution. $\theta(z, t)$ is plotted at times $t \in 0, 0.5, 1, 2, \ldots, 64$ ms. The tilt profiles (solid lines) are dominated by spurious oscillations; the profiles at times $t \in 8, 16$ ms were too oscillatory to show on this graph. (b) Regularized solution, $\lambda = 0.01$. Broad features recognizable as the effect of shear flow are visible (solid lines) compared to the solution where $\lambda \to \infty$ (dashed lines). (c) Experimental and modelled transmission coefficient T'pp at the glass-sample interface. Data (circles) are in good agreement with both an unregularized solution (solid lines) and the solution where $\lambda = 0.01$ (dashes). Agreement with the solution where $\lambda \to \infty$ (dotted lines) is worse.

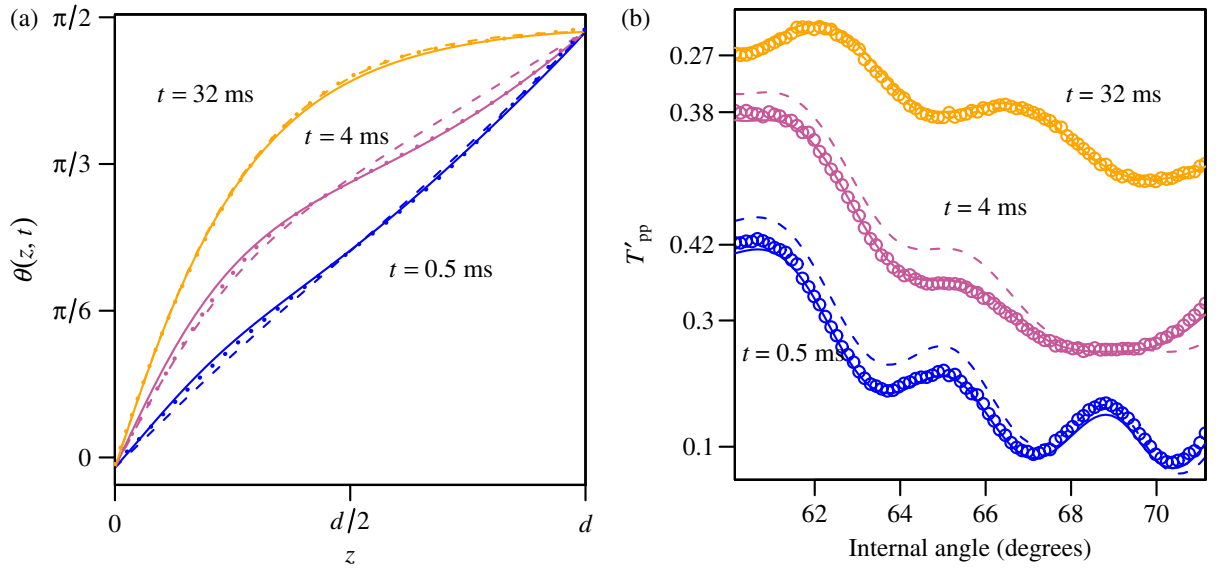

Figure 6. Model results found by solving the Ericksen–Leslie equations. (a) If shear flow is neglected the non-equilibrium tilt profiles (dashes) do not curve toward $\theta = 0$ in the same way as profiles calculated by solving the inverse problem (dots). If shear flow is considered (solid lines) the correct shape is observed. (b) Agreement between the modelled and measured (circles) transmission coefficient is much better when shear flow is taken into account (solid lines) than when it is neglected (dashed lines).

A regularized solution (figure 5(b)), where $\lambda = 0.01$, reveals substantially more about the cell dynamics. Each tilt profile is quite smooth, and again the calculated reflection and transmission coefficients are in good agreement with the observations. The director evolves from the ground state to the switched-on state at a rate which decays with time, which is consistent with (11). Behaviour not explained by (11) is also present: the director rotation near the homeotropic end of the cell is faster than at the mid-plane, and slower at the homogeneous end. Consequently, non-equilibrium tilt profiles curve toward $\theta = \pi/2$ between $z = 0$ and the mid-plane, and toward $\theta = 0$ between the mid-plane and $z = 1$. However, this curving does die out quickly in comparison to the average rate of rotation, so that later tilt profiles are less curved, in broad agreement with (11). The distinctive shape of the director is reminiscent of the backflow effect, where a flow field induced by the rotation of the director acts to speed up re-alignment in some parts of the cell, and slow it down in others. This is an important test, showing that the solution to the inverse problem can differ from the solution to the simplified equations we used to regularize it.

To examine the influence of fluid flow on the director we considered two numerical solutions of the Ericksen–Leslie equations: one in which flow was neglected and a second in which it was taken into account. In both cases, the simplex method of Nelder and Mead [13] was used to find those values for the viscosities which gave the best fit to the experimental data. For the first model the velocity profile is assumed to be zero everywhere, so that just two equations, (3) and (10) need to be solved, and only one of the Leslie viscosities, the rotational viscosity, γ_1, is important. When these equations are solved with $\gamma_1 = 214$ mPa s the resulting non-equilibrium tilt profiles evolve at the correct rate, but have the wrong shape (figure 6(a)), while the reflection and

transmission coefficients (figure 6(b)) are quite different from the experimental measurements. In the second model (3), (4) and (10) were solved, using the values $\gamma_1 = 365$ mPa s, $\alpha_1 = -10$ mPa s, $\alpha_2 + \alpha_3 = -345$ mPa s and $\alpha_4 + \alpha_5 = 350$ mPa s. A much larger value is needed for γ_1 than in the first model because flow induced during the switching process increases the overall rate of re-alignment, reducing the effective rotational viscosity. If that was the only flow-related effect our experiment would not distinguish between the two models, but the flow also alters the shape of the tilt profile, leading to better agreement with the profiles found by solving the inverse problem, and in turn with the experimental data.

6. Conclusions

Although it is a simple matter to predict the reflection and transmission coefficients of a HAN cell measured by the fully-leaky guided-mode technique if the director profile is known, the corresponding inverse problem, reconstruction of the director profile given the measurements, is ill-posed. SVD analysis shows that the experimental error affects the ordinary least-squares problem disproportionately, so that the calculated profiles are dominated by spurious spatial oscillations. Put simply, it is not possible to determine the configuration of the liquid crystal without some additional information. A non-standard form of Tikhonov regularization, inspired by Ericksen–Leslie theory, was introduced to stabilize the problem. To test the modified problem, we determined the time-dependent tilt profile in a HAN cell from experimental data taken after a 3 V_{RMS} ac voltage was applied. A weak backflow effect was recognized in the resulting tilt profiles, even though flow had been neglected in the regularization method, showing that although regularization helps to eliminate implausible solutions it does not restrict the problem unduly. It would have been difficult to decide that fluid flow was important just from an examination of the optical data: it is far easier to decide which physical effects might be important by studying the director profile. In conclusion, the fully-leaky guided mode experiment in conjunction with an approach to regularization based upon simple physics is a powerful tool, capable of extracting detailed information regarding the internal structure of a liquid crystal cell.

Acknowledgments

This work was supported by an EPSRC CASE award in conjunction with HP Labs, Bristol, UK. Thanks are due to Professor W R B Lionheart at the University of Manchester for invaluable advice. GNU R [14] was used for data analysis.

References

[1] Berreman D W 1972 *J. Opt. Soc. Am.* **62** 502
[2] Yang F and Sambles J R 1999 *J. Opt. Soc. Am.* B **16** 488
[3] Jewell S A, Taphouse T S and Sambles J R 2005 *Appl. Phys. Lett.* **87** 1106
[4] Tarantola A 2005 *Inverse Problem Theory and Methods for Model Parameter Estimation* (Philadelphia: SIAM)
[5] Lionheart W R B and Newton C J P 2007 *New J. Phys.* **9** 63
[6] Stewart I W 2004 *The Static and Dynamic Continuum Theory of Liquid Crystals* (London: Taylor and Francis)
[7] Leslie F M 1983 *Phil. Trans. R. Soc. Lond.* A **309** 155

[8] Brochard F, Pieranski P and Guyon E 1972 *Phys. Rev. Lett.* **28** 1681
[9] Wohler H, Haas G, Fritsch M and Mlynsk D A 1988 *J. Opt. Soc. Am.* A **5** 1554
[10] Ko D Y K and Sambles J R 1988 *J. Opt. Soc. Am.* A **5** 1863
[11] Hansen P C 1990 *BIT Numer. Math.* **30** 658
[12] Hansen P C 1992 *SIAM Rev.* **34** 561
[13] Nelder J A and Mead R 1965 *Comput. J.* **7** 308
[14] R Development Core Team 2006 *R: A Language and Environment for Statistical Computing* Online at http://www.R-project.org